Optics Communications 283 (2010) 2835–2840

Contents lists available at ScienceDirect

Optics Communications

journal homepage: www.elsevier.com/locate/optcom

Full-vectorial mode solver for anisotropic optical waveguides using multidomain spectral collocation method

Jinbiao Xiao *, Xiaohan Sun

Laboratory of Photonics and Optical Communications, School of Electronic Science and Engineering, Southeast University, Nanjing 210096, China

ARTICLE INFO

Article history:
Received 7 November 2009
Received in revised form 25 March 2010
Accepted 25 March 2010

ABSTRACT

A full-vectorial mode solver in terms of the transverse magnetic field components for optical waveguides with transverse anisotropy is described by using the multidomain spectral collocation method based on Chebyshev polynomials. The waveguide cross section surrounded by the perfectly matched layers is divided into suitable number of homogeneous rectangles, and then connected with by imposing the continuities of the longitudinal field components at the dielectric interfaces shared by the adjacent rectangles, resulting in a generalized matrix eigenvalue problem. To validate the established method, results of an anisotropic square waveguide and a magnetooptic rib waveguide are presented and compared with those from the full-vectorial finite difference method, full-vectorial beam propagation method, and the experimental data.

1. Introduction

Anisotropic optical waveguides like poling-induced polymer waveguides and magnetooptic waveguides have been widely applied to form various kinds of integrated optical devices, including optical modulators/switches, polarization converters/splitters, and optical isolators [1,2], in photonic integrated circuits or planar lightwave circuits (PICs/PLCs). An efficient and accurate full-vectorial mode solver is indispensable for the analysis and design of these devices. It is almost impossible, however, to get the analytical solutions. Therefore, the use of numerical (or approximate) analysis becomes necessary.

Vectorial coupled mode theory (V-CMT) [2,3] is often used to analyze the magnetooptic waveguides. In V-CMT, the imaginary off-diagonal terms of the relative permittivity tensor are treated by perturbation theory, which is only valid for the waveguide structures where the off-diagonal terms are small compared to the relative permittivity of the corresponding isotropic waveguides [2,3]. Over the years, more rigorously numerical techniques, e.g., finite difference (FD) method [4–7], finite element (FE) method [8–13], and FD- [14,15] and FE-based [16–20] beam propagation method (BPM), have been proposed and successfully applied to analyze the guide modes or the propagation characteristics of the anisotropic dielectric waveguides. However, FD and FE method are often based on the low-order basis functions, normally leading to large matrix.

Alternatively, the series expansion method, e.g., the Galerkin method (GM) and spectral collocation method (SCM), expresses the unknown fields by a complete set of orthogonal basis functions, resulting in a small matrix. The authors have developed a full-vectorial mode solver for optical waveguides with step-index profiles by using the GM with variable transformation technique [21,22]. Although the order of the resulted matrix is small compared to the FD and FE method, it is also time-consuming since laborious integral procedure is required for calculating the matrix elements. In SCM, the unknown fields are imposed to be satisfied with the wave equation at a set of collocation points so that the integral procedure is avoided. As a result, the calculation is more efficient. So far, several kinds of SCM have been proposed and successfully applied in studying the optical waveguide problems. Sharma and Banerjee [23] applied the SCM with single domain to analyze the guided modes and the propagation characteristics of optical waveguides. However, for inhomogeneous waveguide structures, the solutions show the Gibbs phenomenon, resulting in poor convergent behavior. To overcome this problem, Huang et al. [24–27] applied the domain decomposition (DD) technique to the SCM, the so-called multidomain SCM (MSCM), in which the whole interest domain is divided into several homogeneous subdomains, and then connected with by imposing the continuities of the longitudinal field components at the dielectric interfaces. The results [24–27] show that such treatment greatly improves the numerical stability and accuracy. However, the scaling factors of the Laguerre-Gauss basis functions used in the semi-infinite subsomains, which strongly affect the computational accuracy, should be carefully chosen. More recently, Chiang et al. [28,29] proposed a more versatile MSCM, in which a curvilinear coordinate mapping technique is used to transform each curvilinear quadrilateral subdomain into a square one. With the help of this technique, the MSCM can be applied to solve the guided modes of the waveguide structures with curved dielectric interfaces, e.g., circular optical fibers and fused fiber couplers, and compute the band diagrams of the 2-D photonic crystals. Although the MSCM has proved to be powerful and versatile, the

* Corresponding author.
E-mail address: jbxiao@seu.edu.cn (J. Xiao).

0030-4018/$ – see front matter © 2010 Elsevier B.V. All rights reserved.
doi:10.1016/j.optcom.2010.03.057

recent reported studies only focus on the isotropic waveguide structures, in which the anisotropy of the constituent material is completely neglected.

We here describe a full-vectorial mode solver for optical waveguides with transverse anisotropy by using the MSCM in terms of transverse magnetic field components. To avoid the nonphysical reflection from the computational window edges, the robust perfectly matched layer (PML) absorbing boundary conditions [30] are incorporated into the present method. Chebyshev polynomials are chosen as the basis functions for each subdomain because of the nonperiodicity of the waveguide structures [31]. Moreover, additional efforts for choosing the optimum scaling factor as used in [24–26] are avoided since only one kind of polynomials is utilized in our formulation. In order to test the validity and utility of the established method, an anisotropic square waveguide and a magnetooptic rib waveguide are analyzed, and the results are compared with those from the full-vectorial FD method, full-vectorial BPM, and the experimental data.

2. Description of the method

Assuming monochromatic electromagnetic fields with angular frequency ω propagating along the z-direction and using the complex coordinate stretching technique [30], the curl Maxwell's equations can be written as

$$\tilde{\nabla} \times \vec{E} = -j\omega\mu_0 \vec{H} \tag{1a}$$

$$\tilde{\nabla} \times \vec{H} = j\omega\varepsilon_0 \hat{\varepsilon}\, \vec{E} \tag{1b}$$

where ε_0 and μ_0 are the electric permittivity and the magnetic permeability in free space, respectively, and the operator $\tilde{\nabla}$ is defined as

$$\tilde{\nabla} \rightarrow \alpha_x \frac{\partial}{\partial x}\hat{x} + \alpha_y \frac{\partial}{\partial y}\hat{y} + \alpha_z \frac{\partial}{\partial z}\hat{z} \tag{2}$$

where α_x, α_y, and α_z are the complex PML parameters. The parameter α_z is set to be unity since the fields are assumed to propagate along the z-direction. The typical definitions of the other parameters can be found in [30]. Here we consider the dielectric media with transverse anisotropy, and the relative permittivity tensor $\hat{\varepsilon}$ takes the form [1,2]

$$\hat{\varepsilon} = \begin{bmatrix} \varepsilon_{xx} & \varepsilon_{xy} & 0 \\ \varepsilon_{yx} & \varepsilon_{yy} & 0 \\ 0 & 0 & \varepsilon_{zz} \end{bmatrix} \tag{3}$$

From Eqs. (1a) and (1b), a full-vectorial wave equation in terms of magnetic fields can be derived as

$$\tilde{\nabla} \times \left(\hat{\varepsilon}^{-1}\tilde{\nabla} \times \vec{H}\right) - k_0^2 \vec{H} = 0 \tag{4}$$

where $k_0 = 2\pi/\lambda$ with λ being the wavelength in free space. In the case of the optical waveguides with the uniform index profiles along the z-direction, the guided mode solutions can be written as $\vec{H}(x,y)\exp(-j\beta z)$, where $\beta = k_0 n_{\mathrm{eff}}$ is the propagation constant and n_{eff} is the effective index. Using the divergence relation $\tilde{\nabla}\vec{H} = 0$, from Eq. (4) we derive the following coupled eigenvalue equation in terms of the transverse field components H_x and H_y

$$\begin{bmatrix} P_{xx} & P_{xy} \\ P_{yx} & P_{yy} \end{bmatrix} \begin{bmatrix} H_x \\ H_y \end{bmatrix} = \beta^2 \begin{bmatrix} H_x \\ H_y \end{bmatrix} \tag{5}$$

with

$$P_{xx}H_x = \frac{\partial^2 H_x}{\partial \tilde{x}^2} + \varepsilon_{yy}\frac{\partial}{\partial \tilde{y}}\left(\frac{1}{\varepsilon_{zz}}\frac{\partial H_x}{\partial \tilde{y}}\right) + \varepsilon_{yx}\frac{\partial}{\partial \tilde{y}}\left(\frac{1}{\varepsilon_{zz}}\frac{\partial H_x}{\partial \tilde{x}}\right) + k_0^2\varepsilon_{yy}H_x \tag{6a}$$

$$P_{xy}H_y = \frac{\partial^2 H_y}{\partial \tilde{y}\partial \tilde{x}} - \varepsilon_{yy}\frac{\partial}{\partial \tilde{y}}\left(\frac{1}{\varepsilon_{zz}}\frac{\partial H_y}{\partial \tilde{x}}\right) - \varepsilon_{yx}\frac{\partial}{\partial \tilde{x}}\left(\frac{1}{\varepsilon_{zz}}\frac{\partial H_y}{\partial \tilde{x}}\right) - k_0^2\varepsilon_{yx}H_y \tag{6b}$$

$$P_{yx}H_x = \frac{\partial^2 H_x}{\partial \tilde{x}\partial \tilde{y}} - \varepsilon_{xx}\frac{\partial}{\partial \tilde{x}}\left(\frac{1}{\varepsilon_{zz}}\frac{\partial H_x}{\partial \tilde{y}}\right) - \varepsilon_{xy}\frac{\partial}{\partial \tilde{y}}\left(\frac{1}{\varepsilon_{zz}}\frac{\partial H_x}{\partial \tilde{y}}\right) - k_0^2\varepsilon_{xy}H_x \tag{6c}$$

$$P_{yy}H_y = \varepsilon_{xx}\frac{\partial}{\partial \tilde{x}}\left(\frac{1}{\varepsilon_{zz}}\frac{\partial H_y}{\partial \tilde{x}}\right) + \frac{\partial^2 H_y}{\partial \tilde{y}^2} + \varepsilon_{xy}\frac{\partial}{\partial \tilde{x}}\left(\frac{1}{\varepsilon_{zz}}\frac{\partial H_y}{\partial \tilde{y}}\right) + k_0^2\varepsilon_{xx}H_y \tag{6d}$$

where $\partial/\partial\tilde{\gamma} \rightarrow \alpha_\gamma\, \partial/\partial\gamma (\gamma = x,y)$. If the off-diagonal terms in Eq. (3) are set to be zero and the diagonal terms are assumed to be identical, Eq. (5) is reduced to that for the isotropic optical waveguides.

Considering the single domain with constant material parameters, the unknown filed components H_x and H_y are expanded by a set of cardinal basis functions based on the Chebyshev polynomials [31]

$$H_x(x,y) = \sum_{k=1}^{K} H_x^k \Theta_k(x,y) = \sum_{p=0}^{N_x}\sum_{q=0}^{N_y} H_x\left(x_p, y_q\right)\theta_p(x)\theta_q(y) \tag{7a}$$

$$H_y(x,y) = \sum_{k=1}^{K} H_y^k \Theta_k(x,y) = \sum_{p=0}^{N_x}\sum_{q=0}^{N_y} H_y\left(x_p, y_q\right)\theta_p(x)\theta_q(y) \tag{7b}$$

where H_x^k and H_y^k are the values of H_x and H_y, respectively, at the collocation point (x_p, y_q), the so-called Chebyshev Gauss-Lobatto point, N_x+1 and N_y+1 are the number of the collocation points in x- and y-directions, respectively, $K = (N_x+1)\times(N_y+1)$ is the total number of the collocation points, and $\theta_q(x_p) = \delta_{p,q}$ and $\theta_q(y_p) = \delta_{p,q}$ where $\delta_{p,q}$ is the Kronecker delta. The integer quotient function div and the remainder on division function mod are employed to relate k to p and q as

$$p = (k-1)\ \mathrm{div}\left(N_y + 1\right) \tag{8a}$$

$$q = (k-1)\ \mathrm{mod}\left(N_y + 1\right). \tag{8b}$$

Substituting Eqs. (7a) and (7b) into to Eq. (5) together with Eq. (6), and assuring that H_x and H_y are satisfied with Eq. (5) at each collocation point, Eq. (5) is converted into a standard matrix eigenvalue equation as below

$$\begin{bmatrix} A^{xx} & A^{xy} \\ A^{yx} & A^{yy} \end{bmatrix} \begin{bmatrix} H_x \\ H_y \end{bmatrix} = \beta^2 \begin{bmatrix} H_x \\ H_y \end{bmatrix}. \tag{9}$$

The elements of the relative permittivity tensor are constant so that the submatrices A^{xx}, A^{xy}, A^{yx}, and A^{yy} can be derived as follows

$$A^{xx} \rightarrow D^{xx} + \frac{\varepsilon_{yy}}{\varepsilon_{zz}}D^{yy} + \frac{\varepsilon_{yx}}{\varepsilon_{zz}}D^{yx} + k_0^2\varepsilon_{yy}I \tag{10a}$$

$$A^{xy} \rightarrow \left(1 - \frac{\varepsilon_{yy}}{\varepsilon_{zz}}\right)D^{yx} - \frac{\varepsilon_{yx}}{\varepsilon_{zz}}D^{xx} - k_0^2\varepsilon_{yx}I \tag{10b}$$

$$A^{yx} \rightarrow \left(1 - \frac{\varepsilon_{xx}}{\varepsilon_{zz}}\right)D^{xy} - \frac{\varepsilon_{xy}}{\varepsilon_{zz}}D^{yy} - k_0^2\varepsilon_{xy}I \tag{10c}$$

$$A^{yy} \rightarrow \frac{\varepsilon_{xx}}{\varepsilon_{zz}}D^{xx} + D^{yy} + \frac{\varepsilon_{xy}}{\varepsilon_{zz}}D^{xy} + k_0^2\varepsilon_{xx}I \tag{10d}$$

with the matrix elements

$$D^{xx}_{k',k} = \alpha_x(x_{p'}, y_{q'})\left[\alpha_x^{(x)}(x_{p'}, y_{q'})\theta_p^{(x)}(x_{p'}) + \alpha_x(x_{p'}, y_{q'})\theta_p^{(xx)}(x_{p'})\right]\delta_{q',q} \tag{11a}$$

$$D^{yy}_{k',k} = \alpha_y(x_{p'}, y_{q'})\left[\alpha_y^{(y)}(x_{p'}, y_{q'})\theta_q^{(y)}(y_{q'}) + \alpha_y(x_{p'}, y_{q'})\theta_q^{(yy)}(y_{q'})\right]\delta_{p',p} \tag{11b}$$

$$D^{xy}_{k',k} = \alpha_x(x_{p'}, y_{q'})\alpha_y(x_{p'}, y_{q'})\theta_p^{(x)}(x_{p'})\theta_q^{(y)}(y_{q'}) \tag{11c}$$

$$D^{yx}_{k',k} = D^{xy}_{k',k} \tag{11d}$$

where I denotes a identity matrix, the superscripts (γ) and $(\gamma\gamma)$ represent the first and second derivatives, respectively, with respective to γ ($\gamma = x, y$), and k' is related to p' and q' using Eqs. (8a) and (8b).

Now the DD technique is applied to deal with the inhomogeneous waveguide structures for improving the numerical accuracy and stability. The waveguide structures is surrounded by the PMLs, and then divided into suitable number of subdomains with constant material parameters, as shown in Fig. 1. By assembling all the subdomains, we have

$$\begin{bmatrix} A_1 & 0 & 0 & 0 \\ 0 & A_2 & 0 & 0 \\ 0 & 0 & \ddots & 0 \\ 0 & 0 & 0 & A_s \end{bmatrix}\begin{bmatrix} H^1 \\ H^2 \\ \vdots \\ H^s \end{bmatrix} = \beta^2\begin{bmatrix} H^1 \\ H^2 \\ \vdots \\ H^s \end{bmatrix} \tag{12}$$

where A_i and $H^i = \begin{bmatrix} H_x^i \\ H_y^i \end{bmatrix}(i = 1, 2, \cdots, s)$represent the matrix from Eq. (9) and the values of H_x and H_y at the collocation points of the ith subdomain, respectively, and s stands for the total number of the subdomains.

It is noted that the collocation points at the dielectric interfaces are shared by the adjacent subdomains. Instead of Eq. (5), these points are replaced by satisfying the continuity conditions of the longitudinal field components E_z and H_z. From $\tilde{\nabla}\vec{H} = 0$, H_z can be expressed in terms of the transverse field components H_x and H_y as

$$H_z = -\frac{j}{\beta}\left(\frac{\partial H_x}{\partial \tilde{x}} + \frac{\partial H_y}{\partial \tilde{y}}\right) \tag{13a}$$

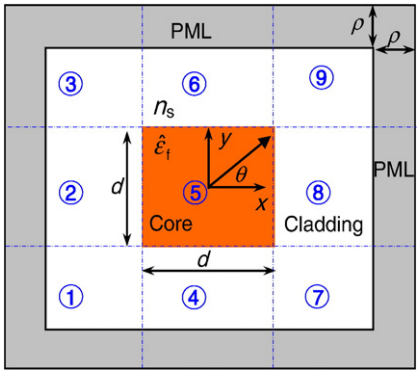

Fig. 1. Cross section of an anisotropic square waveguide surrounded by the PMLs.

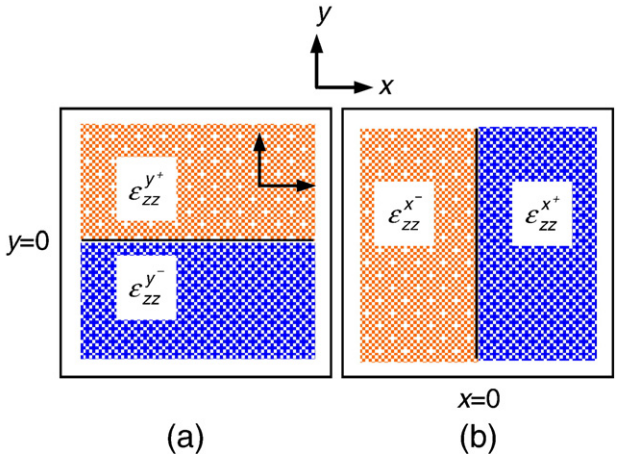

Fig. 2. Horizontal (a) and vertical (b) dielectric interface.

and from Eq. (1b), E_z is expressed by

$$E_z = -\frac{j}{k_0\varepsilon_{zz}}\sqrt{\frac{\mu_0}{\varepsilon_0}}\left(\frac{\partial H_y}{\partial \tilde{x}} - \frac{\partial H_x}{\partial \tilde{y}}\right) \tag{13b}$$

Considering the horizontal interfaces as show in Fig. 2(a), the continuity of E_z gives

$$\varepsilon_{zz}^{y^+}\frac{\partial H_x}{\partial \tilde{y}}\bigg|_{y^-} - \varepsilon_{zz}^{y^-}\frac{\partial H_x}{\partial \tilde{y}}\bigg|_{y^+} = \left(\varepsilon_{zz}^{y^+} - \varepsilon_{zz}^{y^-}\right)\frac{\partial H_y}{\partial \tilde{x}} \tag{14a}$$

and the continuity of H_z yields

$$\frac{\partial H_y}{\partial \tilde{y}}\bigg|_{y^+} = \frac{\partial H_y}{\partial \tilde{y}}\bigg|_{y^-} \tag{14b}$$

where y^+ and y^- denote the locations at the infinitesimally upper and lower side of the horizontal interface, respectively. Similarly, for a vertical interface as show in Fig. 2(b), we have

$$\varepsilon_{zz}^{x^+}\frac{\partial H_y}{\partial \tilde{x}}\bigg|_{x^-} - \varepsilon_{zz}^{x^-}\frac{\partial H_y}{\partial \tilde{x}}\bigg|_{x^+} = \left(\varepsilon_{zz}^{x^+} - \varepsilon_{zz}^{x^-}\right)\frac{\partial H_x}{\partial \tilde{y}} \tag{14c}$$

and

$$\frac{\partial H_x}{\partial \tilde{x}}\bigg|_{x^+} = \frac{\partial H_x}{\partial \tilde{x}}\bigg|_{x^-} \tag{14d}$$

where x^+ and x^- denote the locations at the infinitesimally right and left of the vertical interface, respectively. After all the collocation points at the horizontal and vertical dielectric interfaces are replaced by satisfying the above continuity conditions, Eq. (12) becomes a generalized matrix eigenvalue equation. MATLAB subroutines are employed to solve the finally resulting equation, in which the eigenvectors are related to the modal field distributions, while the corresponding eigenvalues are related to the propagation constants.

3. Numerical results

The validation of the present method is first performed for the anisotropic square waveguide with high index contrast between the core and cladding. The waveguide cross section is surrounded by the PMLs and then divided into nine homogeneous rectangles, as shown in Fig.1. The cladding is set to be isotropic with the index $n_s = 1.0$ (air), whereas the core is set to be anisotropic, a poling-induced polymer.

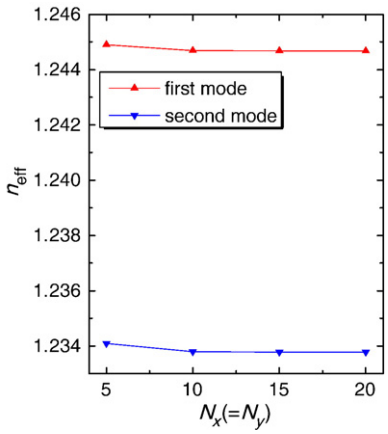

Fig. 3. Effective indices n_{eff} of the two lowest order modes for an anisotropic square waveguide as a function of the degree of the Chebyshev polynomials N_x $(=N_y)$.

For the sake of simplicity, the core is assumed to be homogeneously poled at an angle $\theta=45°$ with respect to the x-axis so that the relative permittivity tensor can be expressed by [1,32,33]

$$\hat{\varepsilon}_f = \begin{bmatrix} n_e^2\cos^2\theta + n_o^2\sin^2\theta & (n_e^2-n_o^2)\cos\theta\sin\theta & 0 \\ (n_e^2-n_o^2)\cos\theta\sin\theta & n_e^2\sin^2\theta + n_o^2\cos^2\theta & 0 \\ 0 & 0 & n_o^2 \end{bmatrix} \tag{15}$$

where $n_e = n_f + \frac{2}{3}\Delta n$, $n_o = n_f - \frac{1}{3}\Delta n$, $n_f = 1.65$ is the index of the core prior to poling, and Δn is birefringence of the core. The width (the height) of the core d is taken as 0.6 μm (operation at single-mode condition prior to poling). The computational window is set to be 4.0×4.0 μm with thickness of the PMLs $\rho=1.0$ μm and the operating wavelength λ is assumed to be 1.30 μm.

To investigate the convergent behavior of the present method, the effective indices n_{eff} of the two lowest order modes for the anisotropic square waveguide with $\Delta n=0.015$ as a function of the degree of the Chebyshev polynomial N_x $(=N_y)$ for each subdomain is illustrated in Fig. 3. It can be seen that the results for both modes approach to the convergent solutions with the increasing of the number of the basis function N_x $(=N_y)$. The convergent solutions can be obtained when $N_x=N_y=15$ is chosen, and the results for both modes almost keep constant for further increasing the number of the basis functions. Fig. 4 presents the variation of the effective indices n_{eff} and their difference Δn_{eff} of the two lowest order modes for the anisotropic square waveguide with the core birefringence Δn, where $N_x=N_y=20$. It can be observed that the effective indices of the first mode linearly increase with the increasing of the core birefringence, whereas the results of the second mode show the opposite behavior. It is also seen that as the core birefringence is increased, the modal birefringence linearly increases as expected. In order to examine the accuracy of the present method, results from the full-vectorial FDM [6] are also plotted in Fig. 4. Our results are good agreement with those from the FDM. However, to obtain the results from this FDM, the number of unknowns is up to 320,000 (the mesh size is $\Delta x=\Delta y=0.01$ μm), whilst the corresponding number of the present method is 2 s(N_x+1) $(N_y+1)=7938$. A HP personal computer with 2.0 GHz CPU speed and 2.0 GB memory size is used to execute our program, and the required CPU time for the present method is nearly 4 times less than that of the FD method. Apparently, the present method is more efficient. Fig. 5 shows the field patterns of the two lowest order modes for an anisotropic square waveguide with $\Delta n=0.015$. It is found that the transverse magnetic field components H_x and H_y for both modes have the amplitudes of the same order. Hence, either scalar or semi-vectorial analysis is inadequate for such waveguide structure since neither of the two transverse components is negligible.

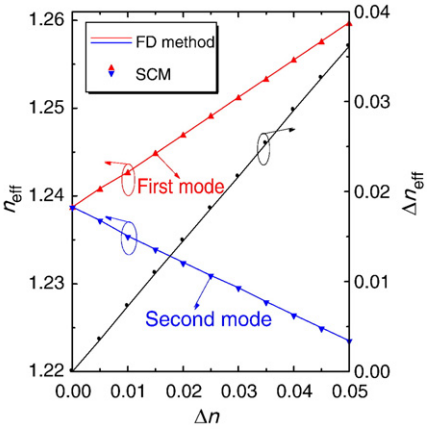

Fig. 4. Variation of the effective indices n_{eff} and their difference Δn_{eff} of the two lowest order modes for an anisotropic square waveguide with the core birefringence Δn.

The present method is also applied to compute the eigenmodes of a magnetooptic rib waveguide as shown in Fig. 6. The waveguide is enclosed by the PMLs and then divided into fifteen subdomains. The waveguide is made of two layers of bismuth yttrium iron garnet (Bi:YIG) with thickness $t_1+h=3.6$ μm and $t_2=3.4$ μm, respectively, grown on a gadolinium gallium garnet (GGG) substrate. The width and height of the rib are, respectively, taken as $w=8.0$ μm and $h=0.5$ μm. When the magnetization is aligned along the z-axis, the relative permittivity tensor of Bi:YIG is given by [2,3]

$$\hat{\varepsilon}_i = \begin{bmatrix} \varepsilon_{xx}^i & j\delta & 0 \\ -j\delta & \varepsilon_{yy}^i & 0 \\ 0 & 0 & \varepsilon_{zz}^i \end{bmatrix} \qquad i=1,2 \tag{16}$$

where ε_{xx}^i, ε_{yy}^i, and ε_{zz}^i are the permittivity tensor terms in the x, y, and z direction, respectively, and δ stands for the first-order magnetooptic effect, which is related to the Faraday rotation angle Θ_F through the refractive index of the magnetooptic medium n by

$$\delta = \frac{n\lambda\Theta_F}{\pi} \tag{17}$$

The introduced magnetooptic effect described by Eq. (16) gives rise to TE-TM mode coupling and thus to mode conversion, which has been applied to form an efficient optical isolator [34]. To get the complete polarization rotation, the effective indices of the fundamental TE- and TM-like modes supported by the unperturbed waveguide $(\delta=0)$ should be identical [3]. With proper device design [34], the stress birefringence caused by the lattice mismatch between the Bi:YIG layers and the GGG substrate Δs can be compensated by the geometric birefringence Δg so that the phase matching condition is realized. According to [34], Δg is set to be 2.2×10^{-4}, and the relative permittivity tensor elements of the Bi:YIG layers are modified as $\varepsilon_{xx}^1=\varepsilon_{zz}^1=(2.19-\Delta g)^2$, $\varepsilon_{yy}^1=(2.19)^2$, $\varepsilon_{xx}^2=\varepsilon_{zz}^2=(2.18-\Delta g)^2$, and $\varepsilon_{yy}^2=(2.18)^2$, with the off-diagonal terms computed assuming $\Theta_F=133°/\text{cm}$. The computational window is set to be 40×11 μm with thickness of the PML $\rho=1.0$ μm. The wavelength is assumed to be 1.485 μm and the number of the basis functions N_x $(=N_y)$ is chosen as 20 for obtaining the convergent solutions.

If the structure is excited with the major component of the fundamental TE-like mode supported by the unperturbed waveguide, mode conversion along the z-axis will occur because of the off-diagonal elements of the relative permittivity tensor. And the TE-like

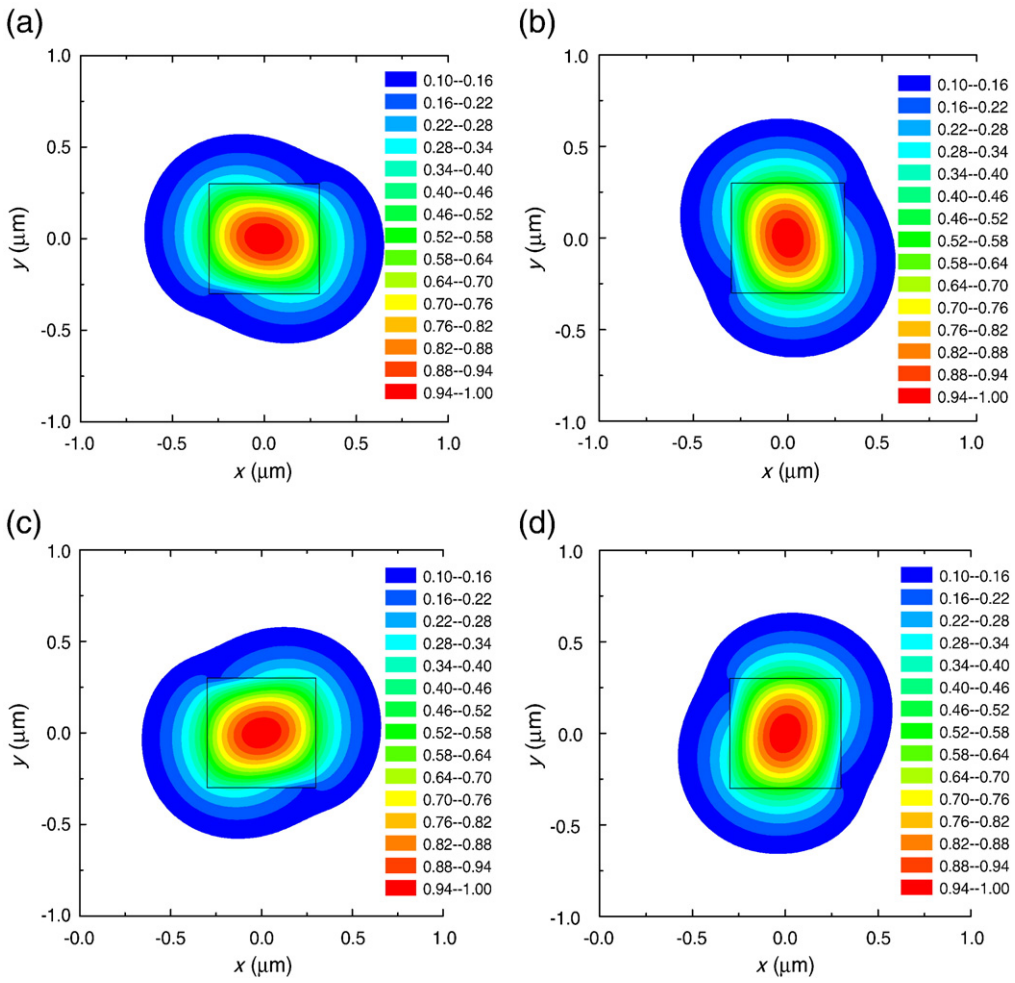

Fig. 5. Field patterns of the eigenmodes for an anisotropic rectangular dielectric waveguide: (a) H_x and (b) H_y for the first mode; (c) H_x and (d) H_y for the second mode.

mode will be converted into TM-like mode after the excited mode propagates a length, the so-called conversion length L_c defined as

$$L_c = \frac{\lambda}{2(n_{eff1} - n_{eff2})} \tag{18}$$

where n_{eff1} and n_{eff2} are the effective indices of the first and second modes of the magnetooptic rib waveguide, respectively. The results computed by the present method are $n_{eff1} = 2.18413227$ and $n_{eff2} = 2.18402319$, respectively, thus the conversion length is $L_c = 6807$ μm, which accords well with the experimental data in [34]. The same structure has also been analyzed by using full-vectorial FD- [15] and FE-BPM [16,18,20], and the results in Refs. [15], [16], [18], and [20] are $L_c = 6800$, 6800, 6780, and 6700 μm, respectively. Our results are also in good agreement with these ones. The values of the transverse magnetic field components H_x and H_y for both modes are complex with nearly equal modulus, but out of phase by $\pm\pi/2$ so that the modes are circularly polarized. In order to better illustrate this, Fig. 7 presents the field patterns of the combinations of the transverse magnetic field components $H_{\pm} = (H_x \pm jH_y)/\sqrt{2}$ of two lowest order modes for the magnetooptic rib waveguide. It is found that the ratio between the amplitudes of H_+ and H_- for the first mode that H_- and H_+ for the second mode is over 30, which indicates that the first and second modes are primarily left- and right-hand circularly polarized, respectively.

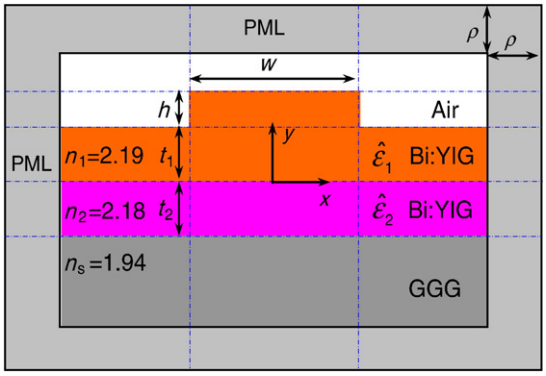

Fig. 6. Cross section of a magnetooptic rib waveguide surrounded by the PMLs.

4. Conclusion

We have developed a full-vectorial mode solver for optical waveguides with transverse anisotropy by using the multidomain spectral collocation method based upon the Chebyshev polynomials. The PML absorption boundary conditions via the complex coordinate stretching technique are incorporated into the present method. The numerical results for an anisotropic square waveguide and a magnetooptic rib waveguide indicate that the established method show superior convergent behavior to the FD method, with high efficiency and accuracy. We here only consider the waveguide structures where the dielectric interfaces are parallel (or perpendicular) with the x- and y-axes. By introducing the curvilinear coordinate mapping technique,

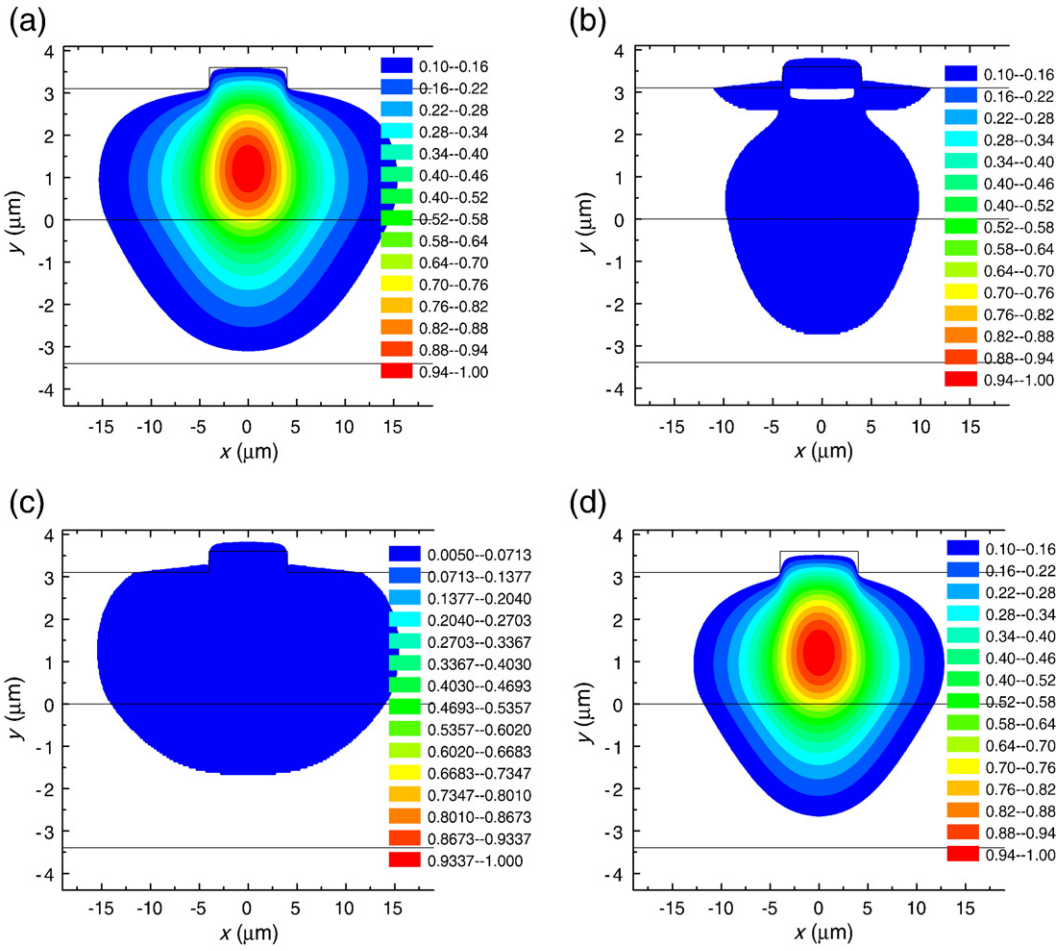

Fig. 7. Field patterns of the combinations of the eigenmodes for a magnetooptic rib waveguide: (a) H_+ and (b) H_- for the first mode; (c) H_+ and (d) H_- for the second mode.

the present method can also be applied to analyze the waveguide structures with curved dielectric interfaces. Moreover, the present method is also attractive to be applied to the full-vectorial BPM in studying the propagation characteristics of the anisotropic dielectric waveguides. Such considerations will be performed in our future work.

Acknowledgements

This work was supported by the Natural Science Foundation of China under Grant 60978005, in part by the Natural Science Foundation of Jiangsu Province of China under Grant BK2007102, in part by the Specialized Research Fund for the Doctoral Program of Higher Education of China under Grant 20060286042, and in part by the Hi-Tech Program of Jiangsu Province of China under Grant BG2007042.

References

[1] J.W. Wu, J. Opt. Soc. Am. B 8 (1991) 142.
[2] H. Dotsch, et al., J. Opt. Soc. Am. B 22 (2005) 240.
[3] M. Loymeyer, et al., Opt. Commun. 158 (1998) 189.
[4] C.L. da Silva Souza Sobrinho, et al., IEE Proc.-H 140 (1993) 224.
[5] P. Lusse, et al., Electron. Lett. 32 (1996) 38.
[6] A.B. Fallahkhair, et al., J. Lightwave Technol. 26 (2008) 1423.
[7] M.Y. Chen, et al., Opt. Express 17 (2009) 5965.
[8] M. Koshiba, et al., J. Lightwave Technol. 4 (1986) 121.
[9] W.C. Chew, et al., IEEE Trans. Microwave. Theory Tech. 37 (1989) 661.
[10] K. Hayata, et al., IEEE Trans. Microwave. Theory Tech. 37 (1989) 875.
[11] Y. Liu, et al., IEEE Trans. Microwave. Theory Tech. 41 (1993) 1215.
[12] F.A. Kastriku, et al., J. Lightwave Technol. 14 (1996) 780.
[13] V. Schulz, IEEE Trans. Microwave. Theory Tech. 51 (2003) 1086.
[14] C.L. Xu, et al., J. Lightwave Technol 12 (1994) 1926.
[15] L.D.S. Alcantara, et al., J. Lightwave Technol. 23 (2005) 2579.
[16] Y. Tsuji, et al., J. Lightwave Technol. 17 (1999) 723.
[17] H.F. Pinheiro, et al., IEEE Photon. Tecnnol. Lett. 12 (2000) 155.
[18] S. Selleri, et al., IEEE J. Quantum Electron 36 (2000) 1392.
[19] K. Saitoh, et al., J. Lightwave Technol. 19 (2001) 405.
[20] J.P. da Silva, et al., J. Lightwave Technol. 21 (2003) 567.
[21] J. Xiao, et al., J. Opt. Soc. Am. B 21 (2004) 798.
[22] J. Xiao, et al., Opt. Commun. 259 (2006) 115.
[23] A. Sharma, et al., Opt. Lett. 14 (1989) 96.
[24] C.C. Huang, et al., J. Lightwave Technol. 21 (2003) 2284.
[25] C.C. Huang, et al., J. Lightwave Technol. 23 (2005) 2309.
[26] C.C. Huang, et al., IEEE J. Sel. Top. Quantum Electron. 11 (2005) 457.
[27] C.C. Huang, J. Lightwave Technol. 27 (2009) 597.
[28] P.J. Chiang, et al., IEEE J. Quantum Electron. 44 (2008) 56.
[29] P.J. Chiang, et al., Phys. Rev. E 75 (2007) 026703.
[30] W.C. Chew, et al., Microwave. Opt. Technol. Lett. 7 (1994) 599.
[31] J.P. Boyd, Chebyshev and Fourier Spectral Methods, Dover, New York, 2001.
[32] M.C. Oh, et al., IEEE J. Quantum Electron. 31 (1995) 1698.
[33] W.Y. Hwang, et al., IEEE J. Quantum Electron. 32 (1996) 1054.
[34] R. Wolfe, et al., Appl. Phys. Lett. 56 (1990) 426.